doi.org/10.36721/PJPS.2024.37.5.REG.939-948.1

Natural sesquiterpene zingiberene exerts ameliorative effects on growth of glioblastoma cells by instigating ROS mediated apoptosis

Talib Hussain[1]*, Ahmed Alafnan[1], Syed Mohd Danish Rizvi[2], Afrasim Moin[2], Sirajudheen Anwar[1], Abd Elmoneim Osman Elkhalifa[3], Amir Mahgoub Awadelkareem[3], Salman Khan[4] and Ahmed Adel Katamesh[2,5]

[1]Department of Pharmacology and Toxicology, College of Pharmacy, University of Hail, Hail, Saudi Arabia
[2]Department of Pharmaceutics, College of Pharmacy, University of Ha'il, Ha'il, Saudi Arabia
[3]Department of Clinical Nutrition, College of Applied Medical Sciences, University of Hail, Ha'il, Saudi Arabia
[4]Nanotechnology and Nanomedicine Lab-6 (IIRC), Department of Biosciences, Integral University, Lucknow, India
[5]Department of Pharmaceutics, Central Administration for Drug Control, Egyptian Drug Authority "EDA", Giza, Egypt

Abstract: Glioblastoma multiforme is the most aggressive and invasive primary brain tumor in adults, and its prognosis and survival rate remain poor. Despite substantial improvements in therapy, the 5-year survival rate of glioblastoma patients remains low. Sesquiterpenes have previously been found to be effective in inhibiting the proliferation and growth of breast, gastric, and lung cancer cells. Owing to their efficacy, sesquiterpenes have been used in various clinical trials. In the present study, we investigated the anticancer efficacy of a well-known sesquiterpene, Zingiberene, isolated from *Zingiber officinale* in C6 glioblastoma cells. Zingiberene suppresses the growth and proliferation of C6 cells. Upon treatment of C6 cells with zingiberene, nuclear fragmentation and ROS were qualitatively enhanced compared to untreated control cells. The levels of caspase-3 were also significantly reduced ($p<0.01$), with a concomitant decline in the mRNA expression of Bax and Bcl-2. On the basis of molecular docking studies, Zingiberene demonstrated good binding energy score of -6.8 and -5.5 Kcal/mol towards Bax and Bcl-2 proteins, respectively. Based on these observations, it was inferred that zingiberene has potential as a plausible therapeutic agent against glioblastoma cells. Detailed mechanistic studies are needed to substantiate and establish the anticancer effects of zingiberene against glioblastoma cells.

Keywords: Zingiberine, glioblastoma multiforme, apoptosis, ROS.

INTRODUCTION

Various bioactive constituents derived from microbes have recently gained attention as plausible anticancer therapeutics, primarily because of their low cytotoxicity (Huang *et al.*, 2021). Plant-derived chemotherapeutics, such as Taxol, are important tools for the clinical management of various types of cancers (Husain *et al.*, 2023). An array of metabolites produced by various plants has been classified into several types based on their structure (Elshafie *et al.*, 2023). Among these, sesquiterpenes are the largest class of bioactive compounds found abundantly in various plants. Sesquiterpenes have previously been found to be effective in inhibiting the proliferation and growth of various cancers (Adekenov *et al.*, 2023). Intriguingly, owing to their efficacy sesquiterpenes have also been used in various clinical trials (Abu-Izneid *et al.*, 2020). Subsequently, these groups of bioactive compounds have also been reported to exhibit several pharmacological activities, including antimicrobial, antioxidant, anti-inflammatory, and anticancer (Togar *et al.*, 2015).

Zingiberene (ZNG) is an important monocyclic sesquiterpene commonly isolated from *Zingiber officinale* (Mao *et al.*, 2019). Previously, *Z. officinale* was shown to impede the growth and proliferation of various types of cancer (Mahomoodally *et al.*, 2021). Nevertheless, there remains significant scope for elucidating the molecular mechanisms underlying the anticancer effects of ZNG.

Glioblastoma multiforme (GBM) is a debilitating form of brain tumor that arises from a preceding astrocytoma or *de novo*. Dauntingly, the North America have been reported for maximum GBM America, followed by Australia, Northern and Western Europe. In the USA alone, the age-adjusted incidence rate of GBM remains at 3.19 per 100,000 persons, with an overall incidence rate of 9.23 per 100,000 persons (Grochans *et al.*, 2022). Indeed, the cumulative incidence rate of central nervous system tumors globally remains high at 6.7 per 100,000 individuals, of which 51% cases are diagnosed with gliomas. Correlating the global pattern with Pakistan was recently reported to be associated with 7097 cases of glioblastoma (Abdullah *et al.*, 2019).

Due to its high rates of vascular and mitotic proliferation and malignancy, GBM is one of the most dreaded forms of brain tumor, as per the World Health Organization (WHO). Furthermore, GBM cases have also been reported to have a low survival rate of approximately 33%

*Corresponding authors: e-mails: md.talib@uoh.edu.sa

(Tiwari *et al*., 2021). Currently, surgical resection of the tumor with concomitant administration of chemotherapeutic temozolomide is the first-line management strategy for patients with GBM. Intriguingly, recent reports have shown an increased interest in exploring the anticancer effects of various natural compounds against glioblastoma (Asma *et al*., 2022; Czarnik-Kwaśniak *et al*., 2019; Cheng *et al*., 2020). In light of this evidence, the authors investigated, for the first time, the efficacy of ZNG for its plausible anticancer effects against rat-derived glioblastoma cells *in vitro*.

MATERIALS AND METHODS

Chemicals

Cell culture reagents, such as DMEM-high glucose medium, antibiotic–antimycotic solution and fetal bovine serum, were procured from Gibco (Thermo Fisher Scientific, USA). The iPurATM Total RNA Miniprep Purification Kit, MTT dye and RNase A were procured from HiMedia (India). 2, 7- dichlorodihydrofluorescein diacetate (DCFH-DA) along 4, 6-diamidino-2-phenylindole (DAPI) were purchased from Sigma, USA.

Methods Cell culture maintenance

Rodent-derived glioblastoma multiforme C6 cells were procured from the National Center for Cell Sciences (NCCS), Pune, India). The cells were maintained in DMEM-high glucose supplemented with 10% fetal bovine serum (FBS) and antibiotic-antimycotic solution (1%). Both FBS and the antimicrobial solution were mixed with the medium at a v/v ratio. The C6 cells were allowed to proliferate at 37°C in an atmosphere containing 5% CO_2.

ZNG mediated cytotoxicity

ZNG-induced cytotoxic effects on C6 cells were evaluated using the MTT assay (Hussain *et al*., 2024). 1×10^4 C6 cells were treated with 20, 40 and 80µM concentration of ZNG for 24h dissolved in DMSO having a concentration of 0.1M for stock solution. After incubation, the cells were treated with 10µl 5mg/mL of MTT dye for 4h. Next, 100µL DMSO was added to each dosed and untreated control C6 group and the 96-well plate was left undisturbed for 30 min. The absorbance of each well was recorded at 570nm using a spectrophotometer (Bio-Rad, USA). The cytotoxic effect of ZNG was determined by calculating the cell viability percentage (%) of C6 cells post-treatment with ZNG using the following formula (Hussain *et al*., 2024), where C6 cells without any exposure to ZNG were used as controls.

$$\text{Cell viability (\%)} \frac{\text{Absorbance of treated C6 cells}}{\text{Absorbance of untreated C6 cells}} \times 100$$

ZNG effects on lactose dehydrogenase (LDH) levels

The ZNG-mediated release of LDH in C6 cells was estimated as previously described, with slight modifications (Ahmad *et al*., 2021). 5×10^4 C6 cells were exposed to 20, 40, or 80µM ZNG and incubated for 24 h, as described above. Subsequently, 100µL of the reaction mixture from the kit (100µL) was mixed with the supernatant collected from each concentration group of ZNG-treated cells and left undisturbed for 30 min. Formazan formation was quantified by recording the absorbance of the different groups at 490 nm using a spectrophotometer (Bio-Rad, USA). The amount of LDH released was proportional to the amount of formazan crystals formed. Cytotoxicity was interpreted as a percentage using the following formula reported earlier (Ahmad *et al*., 2021):

$$\text{Cytotoxicity (\%)} = \frac{\{(\text{ZNG treated LDH Activity}) \ (\text{spontaneous LDH activity})\}}{\{(\text{maximum LDH activity}) \ (\text{spontaneous LDH activity})\}} \times 100$$

ZNG induced oxidative stress

The effects of ZNG on the induction of reactive oxygen species (ROS)-mediated oxidative stress in C6 cells have been previously described (Rizvi *et al*., 2024). The cells (1×10^6 cells were exposed to ZNG for 6h. Cells were exposed to 10µM DCFH-DA for 30 min in the dark. C6 cells exposed to ZNG were analyzed for DCFH-DA-associated green fluorescence using the FLoid Imaging Station (Thermo Fischer Scientific, USA). The levels of green fluorescence in each ZNG-treated C6 cell line were qualitatively compared with those in untreated or control C6 cells.

To quantify ROS levels, C6 cells were exposed to 20, 40, and 80µM ZNG for 6h and stained with DCFH-DA, as described above. DCFH-DA fluorescence was recorded at a wavelength ratio of 485:528 nm (excitation: emission) using a fluorimeter (BioTek, USA). The results were interpreted by expressing the fluorescence intensity percentage of each ZNG-exposed C6 cell line in comparison with that of the untreated control.

Effects of ZNG on nuclear morphology

In this assay, 1×10^4 rat glioblastoma cells were used, as previously described (Rizvi *et al*., 2024). The cells were treated with the indicated ZNG concentrations for 24h and then fixed for 10 min in ice-cold methanol. Subsequently, the cells were stained with freshly prepared 2µg/ml DAPI solution for 30 min in the dark at 37°C. The treated and untreated control cells were then qualitatively visualized for characteristic blue fluorescence using a FLoid imaging station (Thermo Fischer Scientific, USA).

Assessment of caspase-3 activation

Caspase-3 levels in ZNG-treated C6 cells were evaluated colorimetrically, according to a previously published protocol (Shekh *et al*., 2023). 3×10^6 C6 cells were exposed to the indicated concentrations of ZNG for 24 h and centrifuged at 10,000 rpm at 4°C for 1 min. Next, 50µL of supernatant from each group was collected and mixed with an equal volume of reaction buffer. The DEVD-pNA substrate (4mM) was then added to each

treated and untreated control group and the reaction was allowed to proceed for 10min. The absorbance was recorded at 405 nm for the treated and untreated groups using a spectrophotometer (Bio-Rad, USA). The findings were interpreted as the percentage of caspase-3 activity compared with the untreated control.

Effect of caspase-3 inhibitor

The effect of caspase-3 inhibitor pretreatment on ZNG exposure was evaluated using the MTT assay (Ahmad *et al.*, 2023). Initially, 1×10^4 C6 cells were pre-treated with 50μM caspase-3 inhibitor (Z-DEVD-FMK; 50μM) for 2 h. Then, the cells were exposed to the specified ZNG concentrations for the next 24h. Finally, the viability of C6 cells was estimated by quantifying the formation of formazan crystals according to the protocol described in Subsection 2.3.1.

qRT-PCR analysis

1×10^4 C6 cells exposed to the indicated ZNG concentrations for 24h were used in the assay. Isolated total RNA (2μg) was used to synthesize cDNA using a Verso cDNA Synthesis Kit (Thermo Fischer Scientific, USA), following the manufacturer's protocol. The primer sequences used in this study were synthesized using Nick (table 1). qPCR analysis was performed using SYBR Green qPCR kit according to the manufacturer's instructions (Thermo Fisher Scientific, USA) and ABI-7500 real-time PCR (Applied Biosystems; Thermo Fisher Scientific, USA). The comparative cycle threshold or CT value was used to interpolate the differences in gene expression relative to the control gene using the $^{2\Delta\Delta}$CT method, as previously described (Ahmad *et al.*, 2023). GAPDH was used as a housekeeping gene for all calculations.

Docking analysis

ZNG was docked with pro-apoptotic (Bax) and anti-apoptotic (Bcl-2) genes using Auto Dock as described previously (Butt *et al.*, 2020). Protein structures with PDB ID 4S0O and 6GI8 were subsequently modified by omitting the duplicated chains and water molecules. The 3D structure of ZNG was retrieved from the PubChem database. The binding pocket coordinates were selected from the centroid of the target protein and subsequently placed in a 40 × 40 × 40 Å cubic box. Polar hydrogen and Kollman charges are also added. A genetic algorithm, along with the Lamarckian GA, was used to save the output file.

STATISTICAL ANALYSIS

Data obtained during the study are reported as the mean ± SEM of triplicate experiments performed three times. One-way ANOVA (Dunnett's *post hoc* test) was used to determine statistically significant differences between the treated groups and untreated controls using GraphPad Prism (Ver. 5.0). *Represent $p<0.05$, **$p<0.01$ and ***$p<0.001$.

RESULTS

ZNG inhibited the proliferation of C6 glioblastoma cells

A cell proliferation assay was performed to evaluate the growth-suppressive effects of ZNG on C6 cells. ZNG treatment caused dose-dependent suppression of cell proliferation. The cell viability of the C6 cell line was found to be 77.82±3.57%, 57.48±3.87% and 35.48± 3.08% at the indicated doses of 20, 40 and 80μM, respectively (fig. 1A). Therefore, ZNG treatment efficiently inhibited glioblastoma cell proliferation in a dose-dependent manner.

ZNG mediated the LDH release in C6 glioblastoma cells

An lactate dehydrogenase (LDH) release assay was performed to confirm the cytotoxic effects of ZNG on C6 cells. As depicted in fig. 1B, ZNG mediated the release of LDH and it was found to be 31.94±2.86 (20μM). Furthermore, it augmented to 48.71±3.25 and 67.52±4.25 at 40 and 80μM respectively in comparison with untreated control cells. Thus, ZNG treatment mediates LDH release in C6 glioblastoma cells.

ZNG elevated ROS -mediated oxidative stress in glioblastoma cells

DCFH-DA staining was performed to study the effect of ZNG treatment on ROS generation in C6 glioblastoma cells. As shown in fig. 2A, a higher fluorescence intensity was observed at higher doses than in untreated C6 cells. Furthermore, ZNG impelled the generation of ROS in a dose-dependent manner, whereas an elevated intensity of DCFH-DA-mediated fluorescence was observed in C6 cells exposed to 80μM ZNG as compared to the C6 cells treated with either 40 or 80μM ZNG. These results suggest that ZNG increased ROS production in C6 cells.

As shown in fig. 2B, a significant increase in the level of ROS was noticed by 21.38±3.56% in ZNG-treated C6 cells in comparison to the untreated cells. Interestingly, ROS generation of ROS increase to 40.35±3.27% and 55.42±4.49% in C6 cells at the indicated doses of 40μM and 80μM respectively. These results confirm that ZNG treatment elevated ROS generation in C6 glioblastoma cells.

ZNG mediated condensation and fragmentation in the nuclei of C6 glioblastoma cells

DAPI staining was performed to evaluate nuclear alterations in ZNG-treated C6 cells. Untreated cells did not exhibit any substantial changes in the nuclei of the glioblastoma cells (fig. 3). In contrast, ZNG-treated C6 cell nuclei showed significant condensation and fragmentation. Therefore, treatment with ZNG mediates condensation and fragmentation in C6 glioblastoma cells.

ZNG elevated activity of caspase-3

To investigate the effect of ZNG on the activity of caspase-3, glioblastoma cells were cultured with different doses of ZNG. It was observed that ZNG elevated caspase-3 activity to 35.36±4.54% (20µM), 59.46 ± 4.11% (40µM) and 102.58±3.83% (80µM) in comparison with untreated control (fig. 4A).

Additionally, to confirm that apoptosis induction in C6 cells was due to treatment with ZNG, C6 cells were pretreated with a caspase-3 inhibitor (Z-DEVD-FMK) followed by their exposure to ZNG. It was noticed that that preliminary culturing of C6 cells with caspase-3 inhibitor entirely abrogated the apoptosis of C6 cells mediated by ZNG (fig. 4B), indicating that ZNG exposure mediated apoptosis was mediated by increased caspase-3 activity in C6 cells.

Effect of ZNG on mRNA expression levels of apoptotic genes

To delineate the effect of ZNG on the mRNA expression levels of Bcl-2 family members in C6 cancer cells, qRT-PCR was performed. It was found that treatment with various doses of ZNG (20µM, 40µM and 80µM) increased the mRNA expression of Bax (pro-apoptotic) and Bcl2 (anti-apoptotic) genes to 1.19±0.04 (20µM), 1.46±0.05 (40µM) and 1.71±0.06 folds (80µM); 1.27± 0.04 (20µM), 1.56±0.05 (40µM) and 1.81±0.06 folds (80µM) (fig. 5). Thus, it can be concluded that ZNG treatment decreases the expression of anti-apoptotic genes and increases the expression of pro-apoptotic genes.

Molecular docking results

The 2D and 3D structures of ZNG, Bax, and Bcl-2 are shown in fig. 6 and fig. 7, respectively. Our molecular docking results revealed that the binding energy score of ZNG with Bax (pro-apoptotic protein) was -6.8 kcal/mol, as shown in fig. 8. Residues A, Ile31; A, Gln32; A, Ala35; A, Leu45; A, Ala46; A, Leu47; A, Leu125; A, Pro130; A, Glu131; A, Ile133; and A, Arg134 are involved in the molecular docking of ZNG with Bax (fig. 8). However, in the case of molecular docking between ZNG and Bcl-2, the binding energy score was -5.5 kcal/mol. Residues A: Phe104, A: Tyr108, A: Asp111, A: Phe112, A: Met115, A: Val133, A: Leu137 and A: Phe153 were involved in the hydrophobic interactions (fig. 9).

DISCUSSION

Exhaustive investigations over the past several years have established GBM as a dreaded manifestation of brain tumors with a limited scope of surgical resection and concomitant poor survival rate (Aldoghachi *et al.,* 2022). A better understanding of disease pathology has led to improved therapeutic interventions against GBM; however, GBM patients still face the challenge of poor prognosis (Rong *et al*., 2022). Temozolomide (TMZ) remains the first-line therapeutic agent for clinical management of GBM, although its efficacy is not universal. These ambiguous clinical effects of TMZ arise because of the heterogeneity of the malignant and invasive nature of these cancer cells (Cheng *et al*., 2022). This warrants further studies focusing on an in-depth analysis of the mechanisms involved in the pathophysiology of the disease, along with the screening of potential prognostic biomarkers. Intriguingly, it has been hypothesized that bioactive compounds may exhibit efficacy against GBM with relatively low toxicity against normal healthy cells (Ioele *et al*., 2022). Natural bioactive compounds have significant potential for alleviating various dreaded human ailments and are thus being used globally (Rahman *et al*., 2021). The present report focuses on elucidating the anticancer effects of the bioactive sesquiterpene, ZNG, in an in vitro GBM model. ZNG exerted cytotoxic effects against rat glioblastoma C6 cells. It significantly ($p<0.001$) reduced the viability of C6 cells after 24h of exposure. The cytotoxic effects of ZNG corroborated the results of the LDH assay. LDH is an important cellular enzyme that is commonly released into the extra cellular environment after plasma membrane damage. ZNG exposure significantly increased ($p<0.01$) in the LDH concentration in C6 cells. The effect of ZNG on the release of LDH was proportional to the concentration of ZNG. Thus, we conclude that ZNG ameliorated the viability of C6 cells by increasing the release of LDH.

Among several other pathways, apoptosis is an established natural process of cell death through a complex series of molecular events (Cıkla-Suzgun and Kucukguzel, 2019). In addition to its role in the development and differentiation of mammalian cells, apoptosis plays an important role in the host's innate defense mechanisms under various pathological conditions, such as cancer. Apoptosis is an important therapeutic target for formulating an effective therapy against cancer owing to its ability to regulate cell growth and proliferation (Carneiro and El-Deiry, 2020; Sharar and Larisch, 2020). The onset of apoptosis usually begins with nuclear condensation, followed by fragmentation of the genetic material. These specific attributes of apoptosis were observed in C6 cells after ZNG exposure. DAPI-stained photomicrographs revealed alterations in the nuclear morphology of the ZNG-exposed C6 cells.

Similar to their counterparts, ROS are highly unstable reactive species produced by cells during oxidative stress. Reactive oxygen species (ROS) are critical instigators and regulators of cancer cell death. Mounting evidence has not established elevated ROS levels as an important means by which bioactive compounds induce cancer cell death in cancer cells (Nakamura and Takada, 2021). We also found that ZNG exposure substantially increased the ROS generation in C6 cells.

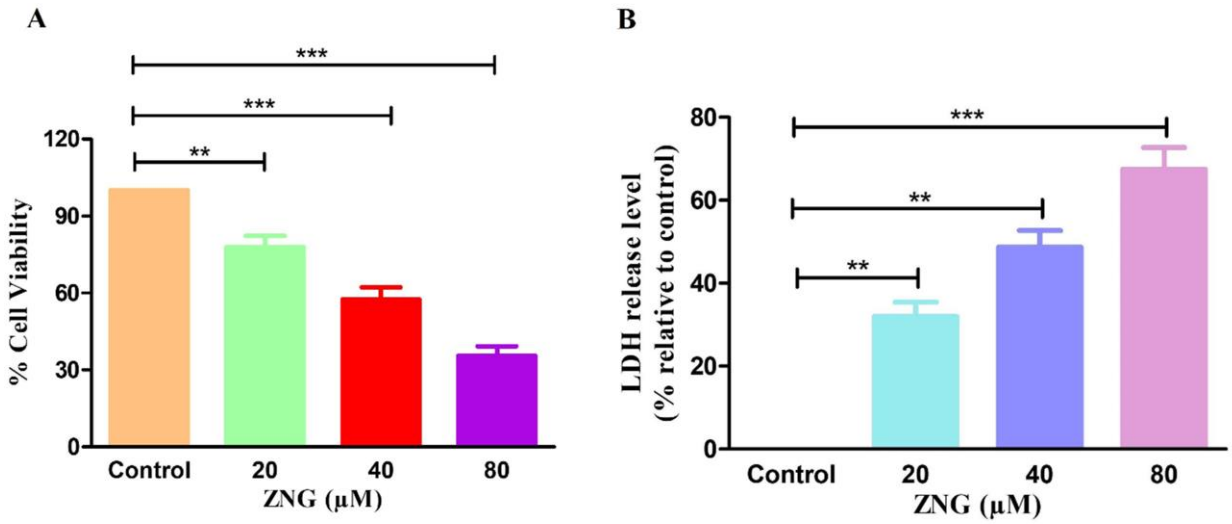

Fig. 1: ZNG mediated cytotoxicity against C6 cells (A) percentage of viable C6 cells post-ZNG treatment and (B) percentage release of LDH from C6 cells after ZNG treatment. **p*<0.05, ***p*<0.01, ****p*<0.001.

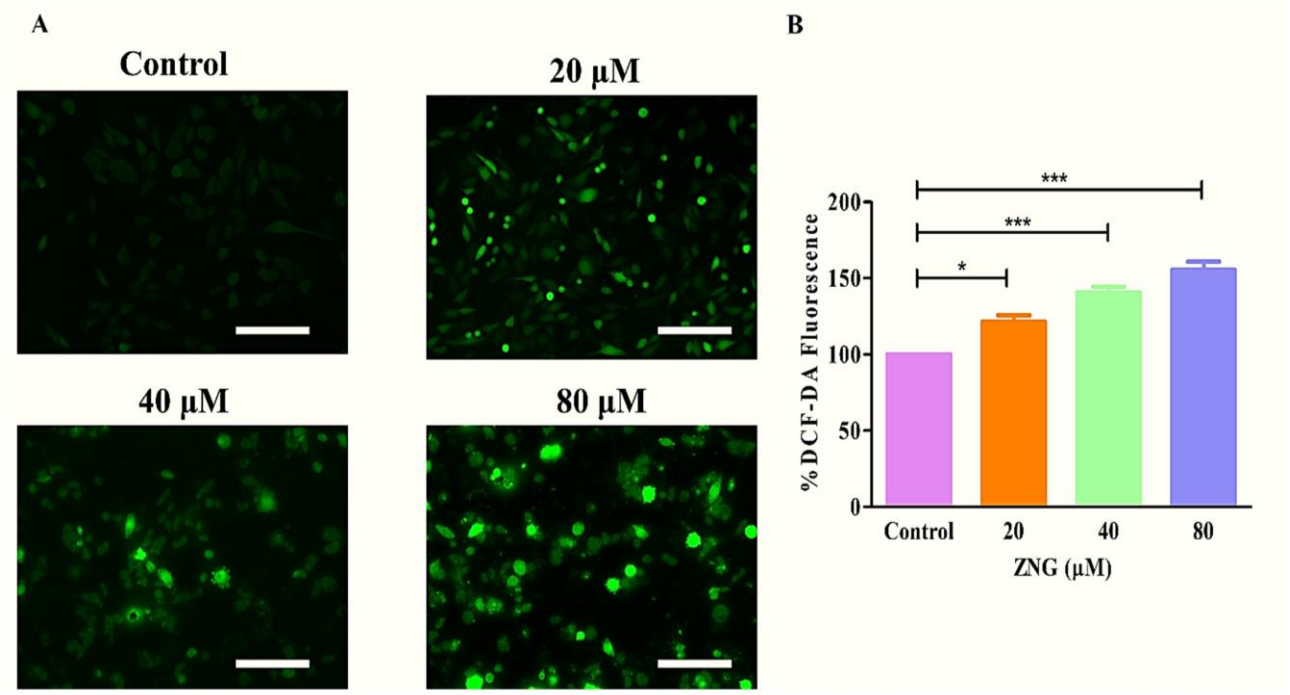

Fig. 2: The efficacy of ZNG in instigating (A) photomicrographs depicting qualitative increase in ROS levels and (B) quantification of intracellular ROS levels within C6 cells. Scale bar = 100µm. **p*<0.05, ***p*<0.01, ****p*<0.001.

Table 1: List of primers used for qPCR.

S. No.	Target gene	Sequence of primers	
		Forward (5'-3')	Reverse (3'-5')
1.	GAPDH	GAAATCCCATCACCATCTTCCAGG	GAGCCCCAGCCTTCTCCATG
2.	Bcl2	GATTGTGGCCTTCTTTGAG	CAAACTGAGCAGAGTCTTC
3.	Bax	GCCCTTTTGCTTCAGGGTTT	TCCAATGTCCAGCCCATGAT

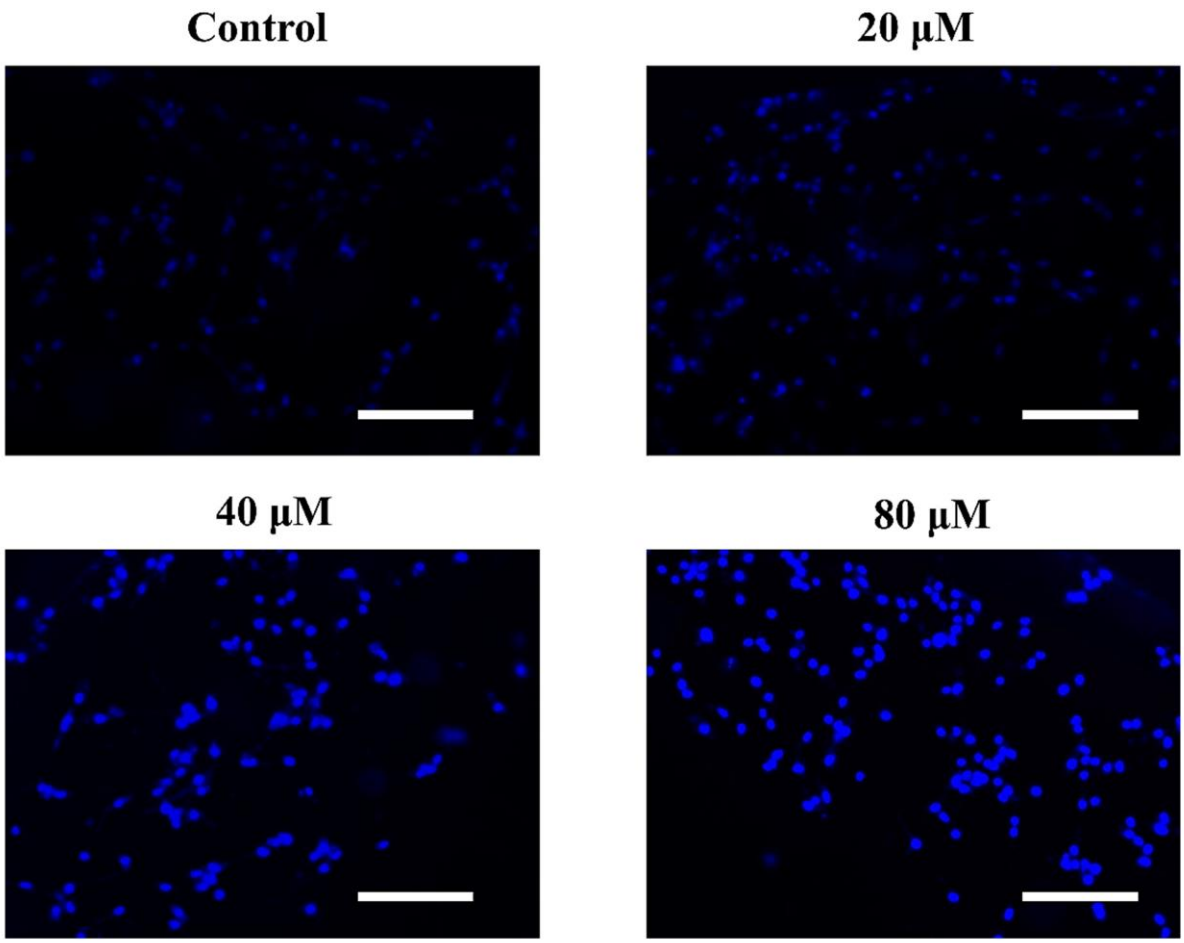

Fig. 3: Initiation of nuclear fragmentation in C6 cells post-ZNG treatment indicated by elevated levels of purple fluorescence proportional to the ZNG concentration. Scale bar = 100 µm.

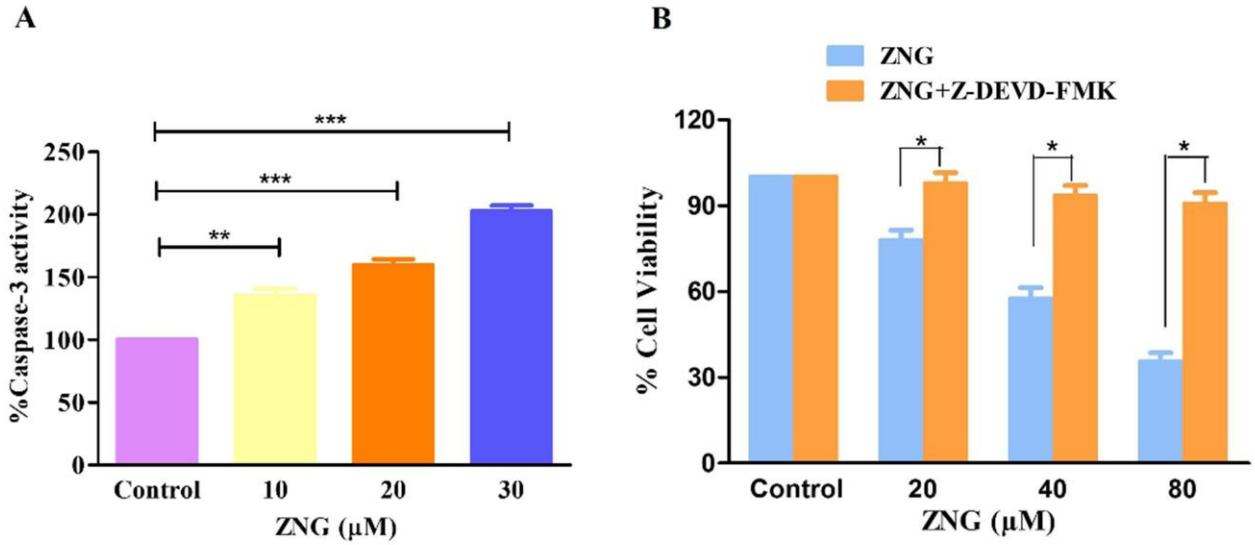

Fig. 4: Activity percentage (%) of (A) caspase-3 in C6 cells post-ZNG treatment and (B) effect of caspase-3 inhibitors on viability of C6 cells. *p<0.05, **p<0.01, ***p<0.001.

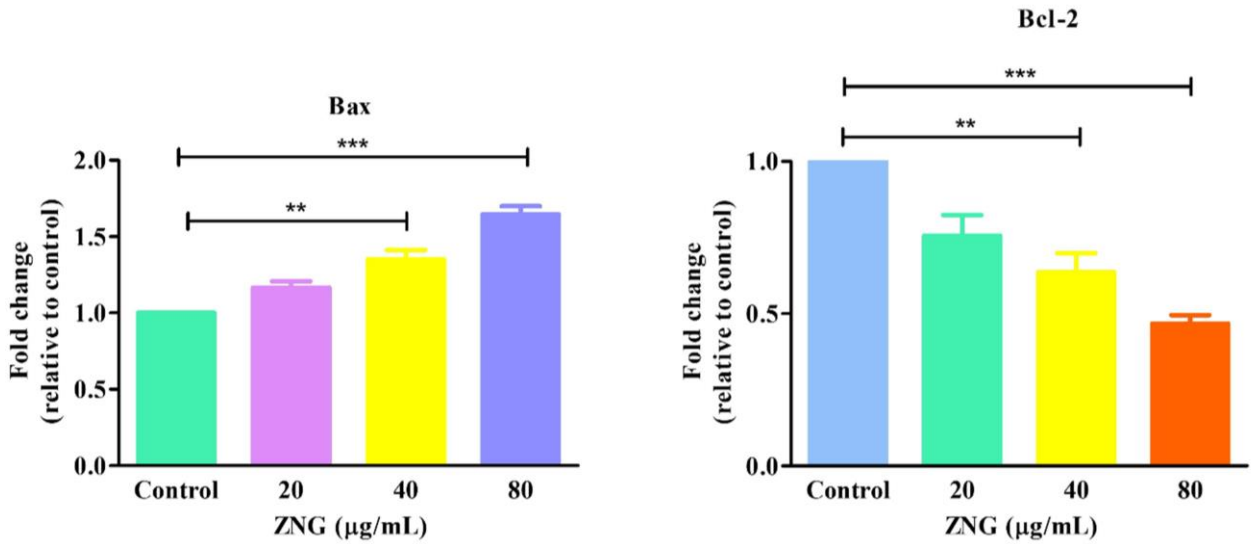

Fig. 5: Real time PCR based fold change evaluation of apoptotic genes mRNA expression in C6 cells exposed to stated ZNG concentrations. *p<0.05, **p<0.01, ***p<0.001.

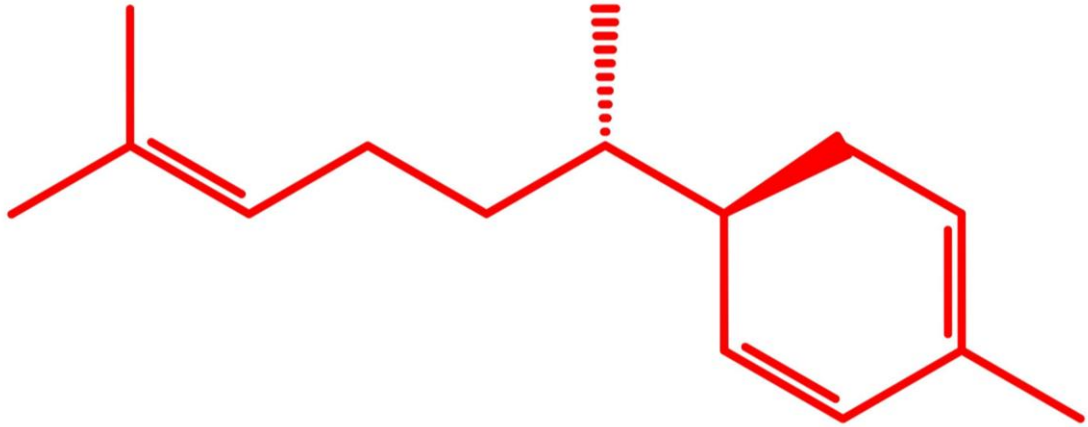

Fig. 6: Two-dimensional structure of ZNG.

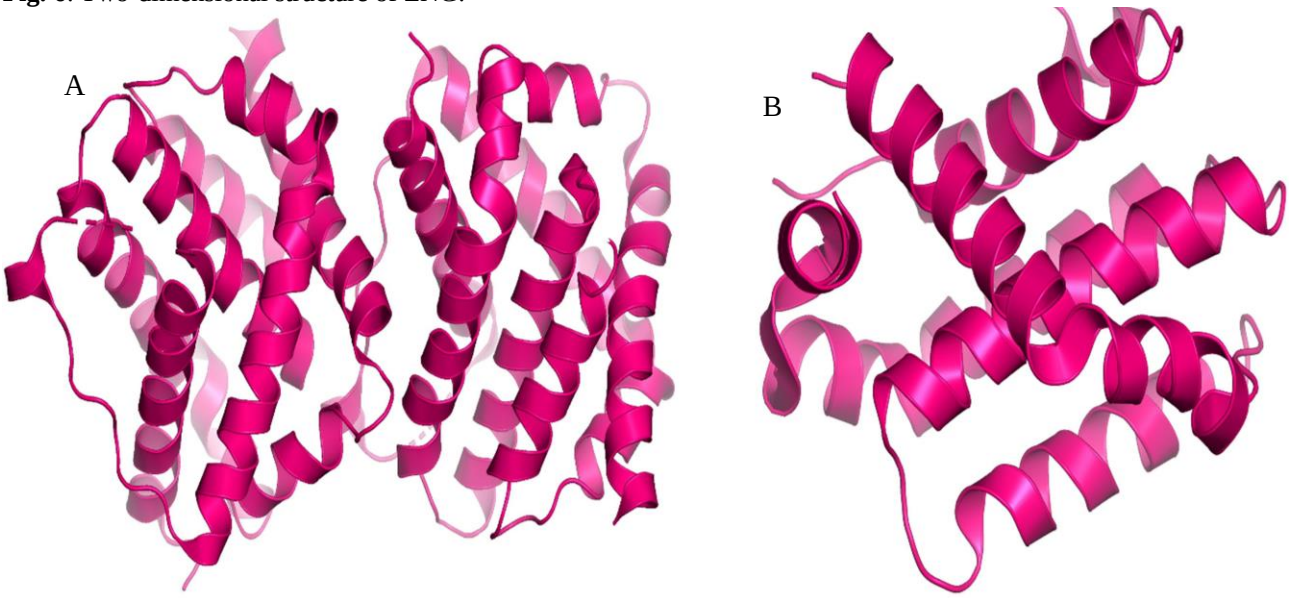

Fig. 7: Three-dimensional structures of key apoptotic proteins (A) Bax and (B) Bcl2

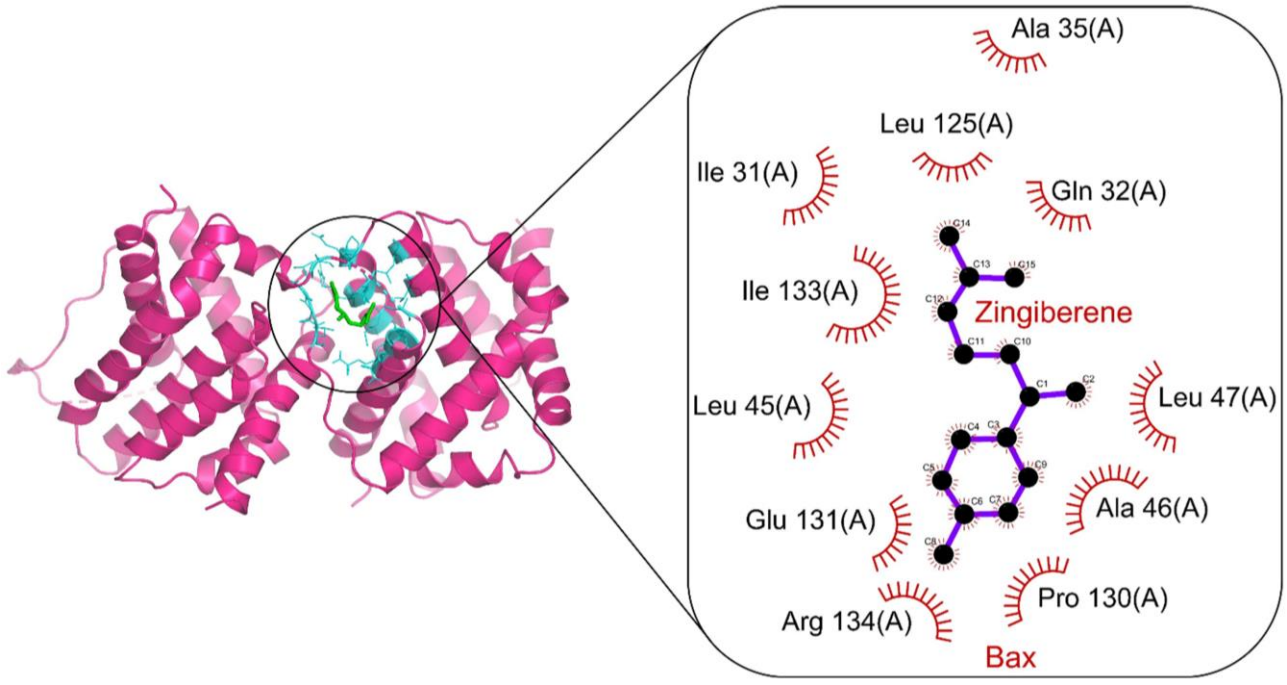

Fig. 8: Ligplot showing molecular interaction between ZNG with pro-apoptotic Bax protein as investigated through Auto Dock Vina.

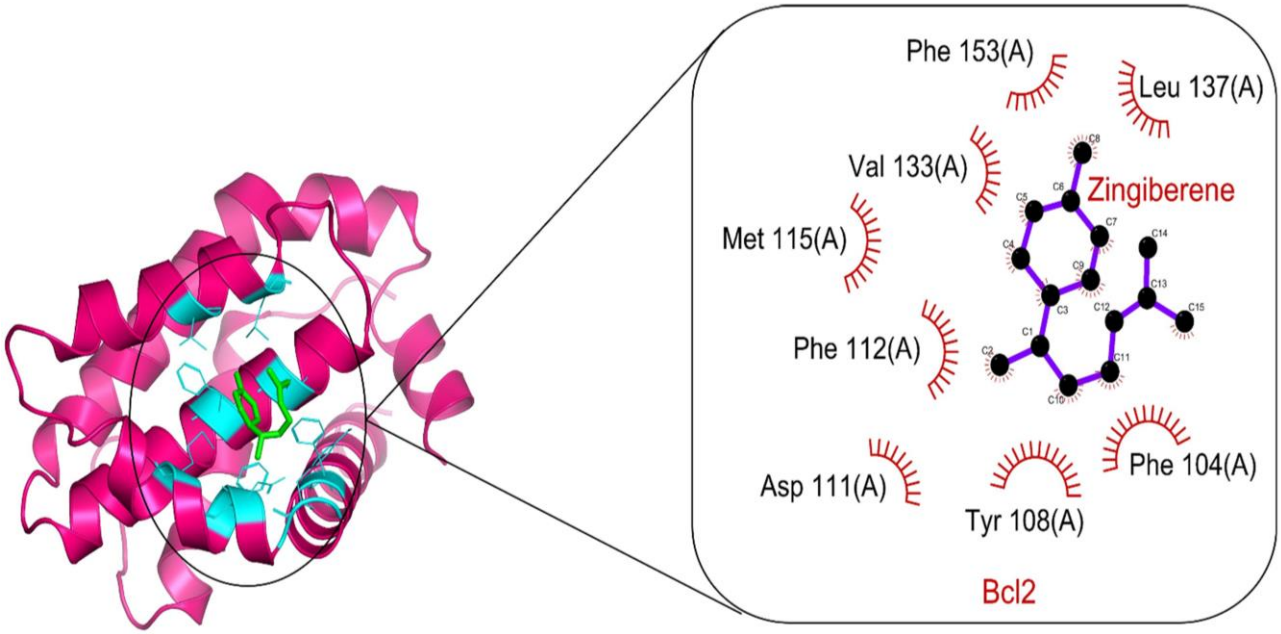

Fig. 9: Ligplot showing molecular interaction between ZNG between ZNG with anti-apoptotic Bcl2 protein as investigated through Auto Dock Vina.

The DCFH-DA-stained photomicrographs indicated an increase in green fluorescence corresponding to ROS generation, which was proportional to the ZNG concentration. This evidence highlights the potential of ZNG as a potent inducer of ROS-mediated oxidative stress, which could have contributed to its cytotoxic effects against C6 cells. Reports have shown that increased ROS generation-mediated apoptotic cell death is commonly associated with reduced mitochondrial viability. The escalation of ROS production usually results in the dissipation of ΔΨm, resulting in loss of function within the mitochondria (Brenner *et al.*, 2024).

An important mode of apoptotic cell death involves caspase activation, which is considered to be an effective member of the cysteine protease family (Han *et al.*, 2023). During our investigation, it was evident that exposure to ZNG led to a considerable increase in the activity of

executioner caspase, caspase-3 (p<0.001). Elevated caspase-3 activity was also found to be proportional to ZNG concentration. During the course of this investigation, we further attempted to elucidate the effect of ZNG-mediated caspase-3 activation on the cytotoxic effects of ZNG against C6 cells using caspase-3 specific inhibitor (Z-DEVD-FMK). The results of this analysis revealed that pre-treatment with C6 significantly increased the viability of glioblastoma cells. This was an important observation to ascertain that the amelioration of ZNG-mediated caspase-3 activation within glioblastoma cells also resulted in significantly reduced cytotoxicity of ZNG. Furthermore, qRT-PCR data showed that ZNG mediated the up regulation of the pro-apoptotic (Bax) gene with a concomitant decrease in the expression of the anti-apoptotic (Bcl-2) gene. The *in vitro* observations in this study further correlated with our *in-silico* findings. The docked complex of ZNG with the pro- and anti-apoptotic proteins, Bax and Bcl-2, respectively, showed significant binding energies.

CONCLUSION

The present study demonstrated the apoptosis-inducing efficacy of ZNG against C6 cells. A more in-depth analysis of these mechanisms is required to fully establish ZNG as a plausible chemotherapeutic agent against GBM. Nevertheless, the observations from this preliminary study conclusively indicated towards the notion that ZNG triggered apoptotic cell death in C6 cells by activating the intrinsic apoptotic pathway. Nevertheless, further in-depth studies are warranted to decipher the molecular mechanism of ZNG to enhance our understanding of its anticancer effects using *in vivo* models.

ACKNOWLEDGEMENT

This research was funded by the Research Deanship of the University of Hail, Hail, Kingdom of Saudi Arabia (Project No.RG-21 167).

REFERENCES

Abdullah UE, Laghari AA, Khalid MU, Rashid HB, Jabbar AA, Mubarak F, Hafiz A, Shamim S and Enam SA (2019). Current management of glioma in Pakistan. *Glioma.*, **2**(3): 139-144.

Abu-Izneid T, Rauf A, Shariati MA, Khalil AA, Imran M, Rebezov M, Uddin MS, Mahomoodally MF and Rengasamy KRR (2020). Sesquiterpenes and their derivatives-natural anticancer compounds: An update. *Pharmacol. Res*., **16**: 105165.

Adekenov S, Spiwok V, Beutler J, Maslova O and Rakhimov K (2023). Cytotoxicity and antitumor activity of arglabin and its derivatives. *Open Access Maced J. Med. Sci.,* **11**(B): 412-420.

Ahmad A, Tiwari RK, Almeleebia TM, Al Fayi MS, Alshahrani MY, Ahmad I, Abohassan MS, Saeed M and Ansari IA (2021). *Swertia chirayita* suppresses the growth of non-small cell lung cancer A549 cells and concomitantly induces apoptosis via downregulation of JAK1/STAT3 pathway. *Saudi J. Biol. Sci*., **28**(11): 6279-6288.

Ahmad A, Tiwari RK, Saeed M, Al-Amrah H, Han I, Choi EH, Yadav DK and Ansari IA (2023) Carvacrol instigates intrinsic and extrinsic apoptosis with abrogation of cell cycle progression in cervical cancer cells: Inhibition of hedgehog/GLI signaling cascade. *Front Chem.,* **10**: 1064191.

Aldoghachi AF, Aldoghachi AF, Breyne K, Ling KH and Cheah PS (2022). Recent advances in the therapeutic strategies of glioblastoma multiforme. *Neuroscience,* **491**: 240-270.

Asma ST, Acaroz U, Imre K, Morar A, Shah SRA, Hussain SZ, Arslan-Acaroz D, Demirbas H, Hajrulai-Musliu Z, Istanbullugil FR, Soleimanzadeh A, Morozov D, Zhu K, Herman V, Ayad A, Athanassiou C and Ince S (2022). Natural products/bioactive compounds as a source of anticancer drugs. *Cancers*, **14**(24): 6203.

Brenner B, Xu F, Zhang Y, Kweon J, Fang R, Sheibani N, Zhang SX, Sun C and Zhang HF (2024). Quantifying nanoscopic alterations associated with mitochondrial dysfunction using three-dimensional single-molecule localization microscopy. *Biomed. Opt. Express*, **15**(3): 1571-1584.

Butt SS, Badshah Y, Shabbir M and Rafiq M (2020). Molecular docking using chimera and autodock vina software for nonbioinformaticians. *JMIR Bioinform. Biotechnol.*, **1**(1): e14232.

Carneiro BA and El-Deiry WS (2020). Targeting apoptosis in cancer therapy. *Nat. Rev. Clin. Oncol*., **17**(7): 395-417.

Cheng AY, Chien YC, Lee HC, Hsieh YH and Yu YL (2020). Water-extracted *Ganoderma lucidum* induces apoptosis and S-phase arrest via cyclin-cdk2 pathway in glioblastoma cells. *Molecules*, **25**(16): 3585.

Cheng Q, Mao L, Huang H, Tang L, Jiang H, Zhang Y, Mu Q (2022). Hesperetin ameliorates glioblastoma by inhibiting proliferation, inducing apoptosis, and suppressing metastasis. *Transl. Cancer Res*., **11**(6): 1781-1794.

Cıkla-Suzgun P and Kucukguzel SG (2019). Recent advances in apoptosis: The role of hydrazones. *Mini Rev. Med. Chem.*, **19**(17): 1427-1442.

Czarnik-Kwasniak J, Kwasniak K, Kwasek P, Swierzowska E, Strojewska A and Tabarkiewicz J (2019). The influence of lycopene, [6]-gingerol, and silymarin on the apoptosis on U-118MG glioblastoma cells *in vitro* model. *Nutrients*, **12**(1): 96.

Elshafie HS, Camele I and Mohamed AA (2023). A comprehensive review on the biological, agricultural

and pharmaceutical properties of secondary metabolites based-plant origin. *Int. J. Mol. Sci.*, **24**(4): 3266.

Grochans S, Cybulska AM, Simińska D, Korbecki J, Kojder K, Chlubek D and Baranowska-Bosiacka I (2022). Epidemiology of glioblastoma multiforme – Literature review. *Cancers*, **14**(10): 2412.

Han JH, Tweedell RE and Kanneganti TD (2023). Evaluation of caspase activation to assess innate immune cell death. *J. Vis. Exp.*, **191**: 10.3791/64308.

Huang M, Lu JJ and Ding J (2021). Natural products in cancer therapy: Past, present and future. *Nat Prod Bioprospect*., **11**(1): 5-13.

Husain A, Meenakshi DU, Ahmad A, Shrivastava N and Khan SA (2023). A review on alternative methods to experimental animals in biological testing: Recent advancement and current strategies. *J. Pharm. Bioallied Sci.*, **15**(4): 165-171.

Hussain T, Alafnan A, Almazni IA, Helmi N, Moin A, Baeissa HM, Awadelkareem AM, Elkhalifa AO, Bakhsh T, Alzahrani A, Alghamdi RM, Khalid M, Tiwari RK and Rizvi SMD (2024). Aloe-emodin exhibits growth-suppressive effects on androgen-independent human prostate cancer DU145 cells via inhibiting the Wnt/β-catenin signaling pathway: An in *vitro* and *in silico* study. *Front Pharmacol*., **14**: 1325184.

Ioele G, Chieffallo M, Occhiuzzi MA, De Luca M, Garofalo A, Ragno G and Grande F (2022). Anticancer drugs: Recent strategies to improve stability profile, pharmacokinetic and pharmacodynamic properties. *Molecules*, **27**(17): 5436.

Mahomoodally MF, Aumeeruddy MZ, Rengasamy KRR, Roshan S, Hammad S, Pandohee J, Hu X and Zengin G (2021). Ginger and its active compounds in cancer therapy: From folk uses to nano-therapeutic applications. *Semin. Cancer Biol*., **69**: 140-149.

Mao QQ, Xu XY, Cao SY, Gan RY, Corke H, Beta T and Li HB (2019). Bioactive compounds and bioactivities of ginger (*Zingiber officinale* Roscoe). *Foods*, **8**(6): 185.

Nakamura H and Takada K (2021). Reactive oxygen species in cancer: Current findings and future directions. *Cancer Sci*., **112**(10): 3945-3952.

Rahman MH, Bajgai J, Fadriquela A, Sharma S, Trinh TT, Akter R, Jeong YJ, Goh SH, Kim CS and Lee KJ (2021). Therapeutic potential of natural products in treating neurodegenerative disorders and their future prospects and challenges. *Molecules*, **26**(17): 5327.

Rizvi SMD, Almazni IA, Moawadh MS, Alharbi ZM, Helmi N, Alqahtani LS, Hussain T, Alafnan A, Moin A, Elkhalifa AO, Awadelkareem AM, Khalid M and Tiwari RK (2024). Targeting NF-κB signaling cascades of glioblastoma by a natural benzophenone, garcinol, via *in vitro* and molecular docking approaches. *Front. Chem*., **12**: 1352009.

Rong L, Li N and Zhang Z (2022). Emerging therapies for glioblastoma: Current state and future directions. *J. Exp. Clin. Cancer Res*., **41**(1): 142.

Shahar N and Larisch S (2020). Inhibiting the inhibitors: Targeting anti-apoptotic proteins in cancer and therapy resistance. *Drug Resist. Updat.*, **52**: 100712.

Shekh R, Ahmad A, Tiwari RK, Saeed M, Shukla R, Al-Thubiani WS, Ansari IA, Ashfaque M and Bajpai P (2023). High therapeutic efficacy of 5-fluorouracil-loaded exosomes against colon cancer cells. *Chem Biol Drug Des*., **101**(4): 962-976.

Tiwari RK, Moin A, Rizvi SMD, Shahid SMA and Bajpai P (2021). Modulating neuroinflammation in neurodegeneration-related dementia: Can microglial toll-like receptors pull the plug? *Metab. Brain Dis*., **36**(5): 829-847.

Togar B, Turkez H, Tatar A, Hacimuftuoglu A and Geyikoglu F (2015). Cytotoxicity and genotoxicity of zingiberene on different neuron cell lines *in vitro*. *Cytotechnology*, **67**(6): 939-946.